

Optimization-Oriented Design of RF/Microwave Circuits Using Inverse-Linear-Input Neuro-Fuzzy-Output Space Mapping with Two Different Dimensionality Simulators

Juan Hinojosa, Fernando Daniel Quesada-Pereira, M. Martínez-Mendoza, and Alejandro Alvarez-Melcón, *Senior Member, IEEE*

Abstract— In this paper, an efficient optimization technique aligning three-dimensional (3D) electromagnetic simulator responses with two-dimensional (2D) electromagnetic simulator responses around space mapped solution, for the electromagnetic design of radiofrequency and microwave 3D circuits is presented. The interface between 2D and 3D electromagnetic simulators is obtained from an inverse linear input space-mapping approach and an output modeling process based on a fuzzy logic technique. It is shown that the technique provides a highly accurate estimation of the 3D design parameter space of the 3D radiofrequency and microwave circuits to be designed, for initially fixed design specifications. Designs of first-order, second-order and sixth-order C-band 3D evanescent rectangular waveguide bandpass filters with dielectric posts show the performance of our approach.

Index Terms—CAD, fuzzy logic, circuit optimization, RF/microwave filters, waveguide filters.

I. INTRODUCTION

IN the aerospace industry, the main constraints over the microwave components concern the mechanical and electrical characteristics. Since the first satellite launch, the challenges have been the reduction in weight and volume, and the performance improvements. To meet the increasing demand over enhanced microwave components, accurate CAD tools have been required. Nowadays, a large range of two-dimensional (2D) and three-dimensional (3D) electromagnetic (EM) simulators are available [1]-[3]. From a computational point of view, the 3D EM simulators are very accurate for the analysis of arbitrary 3D structures, but usually very time-consuming. The 2D EM simulators typically provide efficient and accurate analysis of 2D structures, due to

the reduction of one spatial dimension. However, these 2D structures find fewer applications, because from a practical point of view, many component structures of interest for the space sector are 3D. In this context, we want to focus this work in a design process of 3D RF/microwave circuits by using the efficient capabilities for the numerical modeling of 2D structures.

This design process can be successfully achieved by using a powerful computational optimization tool between the 2D and 3D EM simulators, which adjusts the 2D and 3D dimensions of the RF/microwave circuits in order to meet the design specifications. Many EM-based CAD tools and optimization techniques are available in the literature [4]-[15]. In computational electromagnetics, the trend is to combine different EM theories into hybrid techniques by expanding their capabilities and their efficiency. Among the optimization techniques, the space mapping approach has attracted our interest because of the possibility of reducing the computational time of the EM-based design process. This approach employs two models: a fine model and a coarse model. The fine model is accurate and slow in computational time, whereas the coarse model is fast but less accurate. The concept of the space mapping consists in aligning the space of the design parameters of the fine model with a mapped space of the design parameters of the coarse model by using an optimization tool. The optimization is done using only the efficient coarse model; the fine model is used only a few times during the design process.

For the analysis and design of microwave circuits, artificial neural networks and fuzzy logic techniques have also been employed extensively [16]-[21]. The basic approach consists of training an artificial neural network or a fuzzy logic system over a certain region of interest, and then applying analysis and optimization techniques to the computationally inexpensive extracted models. The use of space-mapping-based neural models and space-mapping-based fuzzy models was demonstrated in [22] and [23], respectively. These works developed a neural-mapping and a neuro-fuzzy-mapping for the input design parameters with a high generalization ability.

In this paper, we describe an innovate interface between 2D and 3D EM simulators for the efficient optimization-oriented design of RF/microwave circuits using inverse-linear-input

Manuscript received January 19, 2010; revised May 27, 2010. This work was supported by Ministerio de Educación y Ciencia of Spain (TEC2007-67630-C03-02/TCM).

Authors are with Universidad Politécnica de Cartagena, Cartagena (Murcia) 30202, Spain. J. Hinojosa is with the Department of Electronics and Computer Engineering (e-mail: juan.hinojosa@upct.es). F. D. Quesada Pereira, M. Martínez-Mendoza and A. Alvarez-Melcon are with the Department of Communications and Information Technologies.

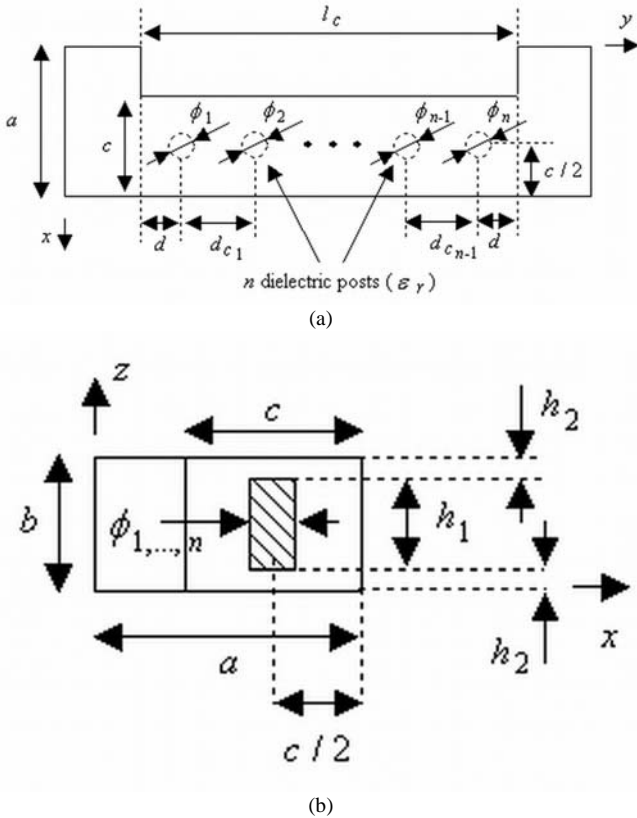


Fig. 1. N th-order evanescent rectangular waveguide bandpass filter with n dielectric posts. (a) Top view. (b) Cross-section view.

neuro-fuzzy-output space-mapped (ILINFO-SM) models. The key idea is to find a mapping from the 2D structure to the final 3D structure. With respect to other space mapping approaches of 3D structures [24]-[28], the highly accurate estimation of the 3D design parameter space is realized from the following two main contributions: 1) An inverse linear input mapping P from the coarse model space (2D EM simulator) to the fine model space (3D EM simulator) is iteratively built by applying a linear iterated prediction method, as described in [28], [29]; 2) the building of a nonlinear output space mapping based on a neuro-fuzzy modeling process [30]-[32]. This neuro-fuzzy output mapping reduces the residual error between the coarse (2D structure) and fine (3D structure) models, and facilitates further optimizations and interpolations, which can not be carried out with an inverse linear input mapping as in [28]. This neuro-fuzzy interpolator idea is related with a neural output space mapping introduced in [27], but in that work the technique is not applied to the interface between 2D and 3D EM simulators.

Our initial approach in [28] is extended and improved in different ways. A neuro-fuzzy-output mapping is added to the inverse-linear-input mapping. The different sub-processes of the ILINFO-SM approach are formulated, described and illustrated by using an example. The accuracy improvement and the interpolation abilities of the whole system are demonstrated. Finally, a step-by-step procedure is proposed for the application of the novel technique to the design of higher order microwave filters. A sixth-order microwave filter is for the first time designed using the proposed approach.

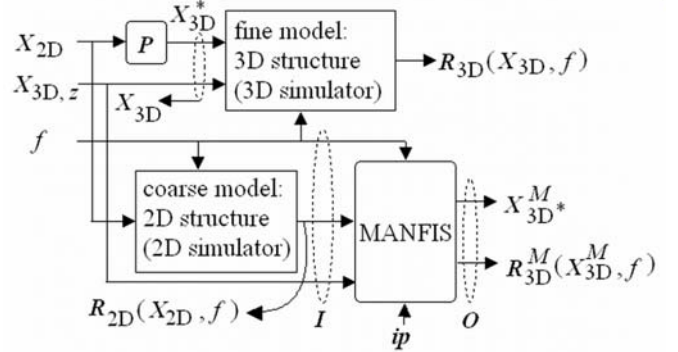


Fig. 2. Inverse-linear-input neuro-fuzzy-output space-mapping approach (MANFIS is the multiple adaptive neuro-fuzzy inference system).

Among the different technologies of interest in the aerospace industry [33], [34], we have opted by evanescent rectangular waveguide filters with dielectric resonators (Fig. 1). The dielectric resonators are dielectric circular posts centered and suspended inside the evanescent rectangular waveguide sections for the 3D structures (non-inductive discontinuities, see Fig. 1(b)), whereas for the 2D structures, the dielectric circular posts touch the top and bottom metallic walls of the evanescent rectangular waveguide sections (inductive discontinuities). The analyses of the 2D and 3D structures are provided by a specific in-house simulator and a commercial tool (HFSS), respectively. The specific in-house simulator is based on an integral equation technique customized for the analysis of 2D inductive discontinuities in rectangular waveguides [3]. To exploit the 2D symmetry of the problem, Green's functions of infinite line-sources inside a parallel plate waveguide are used. On the contrary, HFSS is a full-wave EM field simulator for arbitrary 3D passive circuit analysis. It employs the finite element method and adaptive meshing to solve the 3D EM problems. The integral equation simulator is very fast, since it exploits the 2D symmetry of the problem. On the contrary, the HFSS simulator is slower, since it has to perform a full-wave analysis and a volume mesh of the complete 3D structure.

II. INVERSE-LINEAR-INPUT NEURO-FUZZY-OUTPUT SPACE-MAPPING METHOD

The proposed ILINFO-SM approach is illustrated with the design example of a first-order 3D evanescent rectangular waveguide bandpass filter containing one dielectric post. The unique dielectric post (Fig. 1) is centered in the evanescent waveguide section (l_c). The input/output waveguides are of standard WR-229 type, with dimensions $(a, b) = (58.1, 29.05)$ mm. The fixed design parameters are: $c = 31.1$ mm (the width of the evanescent waveguide section), $h_1 = 18.05$ mm (the height of the dielectric post with $h_2 = 5.5$ mm) and $\epsilon_r = 4$ (the permittivity of the dielectric post). The parameters to be optimized are the diameter of the post (ϕ) and the length of the evanescent waveguide section (l_c).

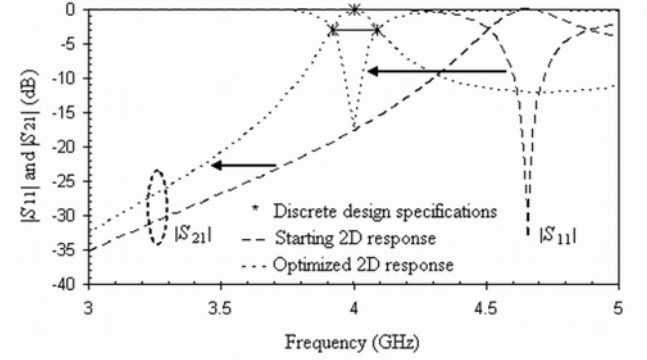
Our proposed ILINFO-SM strategy is illustrated in Fig. 2. The *-symbol has been used to denote the variables that will

be affected by the mapping between 2D and 3D spaces. \mathbf{X}_{2D} , \mathbf{X}_{3D}^* and \mathbf{X}_{3D} are, respectively, optimal 2D, 3D* and 3D design parameter space vectors obtained for initially fixed design specifications ($\mathbf{X}_{2D}, \mathbf{X}_{3D}^* \in \mathfrak{R}^n$ and $\mathbf{X}_{3D} \in \mathfrak{R}^{n+k}$, n and $n+k$ are the numbers of the design parameters in the 2D space (x, y) and in the 3D space (x, y, z) , respectively). \mathbf{X}_{3D}^* has the same order than \mathbf{X}_{2D} . $\mathbf{X}_{3D,z}$ includes the variables of the third dimension (z -axis in Fig. 1), which are known or fixed by constraints. \mathbf{R}_{2D} and \mathbf{R}_{3D} are the corresponding 2D and 3D simulator response vectors and f is the frequency. $\mathbf{P} \in \mathfrak{R}^n$ is the 2D to 3D* mapping vector.

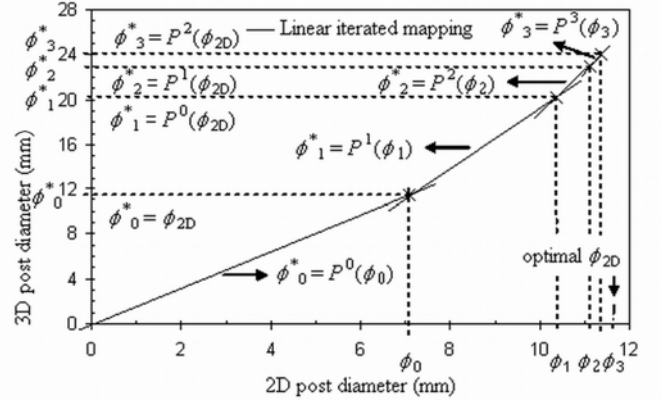
In the example of the first-order bandpass filter (Fig. 1 with one dielectric post), the 2D structure (coarse model) considers the dielectric post as being an inductive discontinuity. The space is reduced to the plane (x, y) , since the field is constant along the z -axis. The 3D structure (fine model) processes a true 3D dielectric post inside the waveguide, where the height of the dielectric post is smaller than the height of the waveguide ($h_1 = 18.05$ mm). The 2D and 3D* design parameter spaces to be optimized according to initially fixed design specifications are $\mathbf{X}_{2D} = [l_c \ \phi]^T$ and $\mathbf{X}_{3D}^* = [l_c^* \ \phi^*]^T$, respectively. In this case, the third dimension is formed by the fixed height of the dielectric post $\mathbf{X}_{3D,z} = h_1 = 18.05$ mm. In this example, we can observe that the numbers of the design parameters in the 2D space (x, y) and in the 3D space (x, y, z) are $n = 2$ and $n+k = 3$ ($k = 1$), respectively.

In our approach, the mapping function \mathbf{P} is linear. Therefore, in most practical cases, the 3D response $\mathbf{R}_{3D}(\mathbf{X}_{3D}^*, \mathbf{X}_{3D,z}, f)$ slightly varies from $\mathbf{R}_{2D}(\mathbf{X}_{2D}, f)$, because of a residual error that can not be eliminated with a linear mapping \mathbf{P} . To solve this problem, we have added a multiple adaptive neuro-fuzzy inference system (MANFIS) [30]-[32] after the 2D EM simulator (Fig. 2). MANFIS, whose internal parameter vector is defined from $\mathbf{i}p$ (premise and consequent parameters), is trained to learn stipulated input-output data pairs obtained during the successive iterations performed to find the mapping \mathbf{P} with the linear prediction method. During the training process of the MANFIS, the inputs are $\mathbf{X}_{3D,z}$ and the discrete design specifications derived from $\mathbf{R}_{2D}(\mathbf{X}_{2D}, f)$. The outputs are \mathbf{X}_{3D}^* and the discrete design specifications extracted from $\mathbf{R}_{3D}(\mathbf{X}_{3D}^*, \mathbf{X}_{3D,z}, f)$.

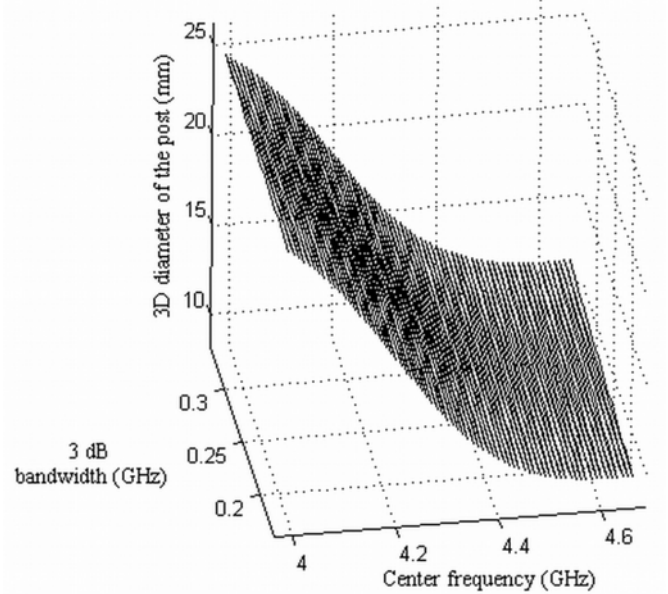
Once MANFIS is trained, we can use it to perform an accurate computation over the 3D* design parameters ($\mathbf{X}_{3D}^M = \mathbf{P}(\mathbf{X}_{2D})$), so that the residual error between $\mathbf{R}_{3D}^M(\mathbf{X}_{3D}^M, \mathbf{X}_{3D,z}, f)$ and $\mathbf{R}_{2D}(\mathbf{X}_{2D}, f)$ is reduced for the initially fixed discrete design specifications (Fig. 2). The consideration of $\mathbf{X}_{3D,z}$ in the MANFIS inputs will facilitate further optimizations and interpolations. The interpolation



(a)



(b)



(c)

Fig. 3. Illustration of the three sub-processes of our proposed approach for the first-order bandpass filter (Fig. 1 with one dielectric post). (a) First sub-process: Target response of the 2D simulator according to the predefined discrete 2D design specifications. (b) Second sub-process: Linear iterated prediction 2D to 3D* space mapping optimization for ϕ . (c) Third sub-process: Output neuro-fuzzy mapping for ϕ .

results will allow to reduce the computational cost of linear iterated prediction 2D to 3D space mapping optimizations by

decreasing the number of 3D simulations necessary to obtain solutions of \mathbf{X}_{3D}^* .

The proposed ILINFO-SM approach consists of three sub-processes, which are illustrated in Fig. 3 for our example (applied only to the diameter of the post (ϕ) for the sake of space): 1) find a target response $\mathbf{R}_{2D}(\mathbf{X}_{2D}, f)$ according to the initially fixed discrete design specifications by optimizing the coarse model, which is the 2D structure (Fig. 3(a)); 2) find \mathbf{X}_{3D}^* of the 3D structure (fine model) and \mathbf{P} by means of an inverse linear input space-mapping optimization (Fig. 3(b)); and 3) develop the output neuro-fuzzy mapping (modeling process) using the MANFIS with stipulated input-output data pairs to obtain accurate 3D* design parameters ($\mathbf{X}_{3D^*}^M$) (Fig. 3(c)). These sub-processes are described and illustrated in the following sub-sections. A space mapping notation similar to [26] is followed. For the example of the first-order bandpass filter (Fig. 1 with one dielectric post), we have used a set of discrete 2D design specifications (f_{2D} , B_{2D}): center frequency $f_{2D} = 4$ GHz and 3 dB bandwidth $B_{2D} = 0.16$ GHz. The optimization task consists in finding the final 3D structure that meets these two predefined 2D design specifications.

A. 2D Model Optimization

The algorithm starts by optimizing the 2D model according to the initially fixed discrete design specifications

$$\mathbf{X}_{2D} = \arg \min_{\mathbf{x}_{2D}} U(\mathbf{R}_{2D}(\mathbf{x}_{2D}, f)) \quad (1)$$

where $\mathbf{R}_{2D} \in \mathfrak{R}^h$ denotes the response vector of the 2D model for h frequency points, U corresponds to the objective function with the initial discrete 2D design specifications (center frequency, bandwidth), $\mathbf{x}_{2D} \in \mathfrak{R}^n$ is the 2D design parameter vector and $\mathbf{X}_{2D} \in \mathfrak{R}^n$ is the optimal 2D design parameter vector to be achieved, which is assumed to be unique. The optimization of the 2D model can be performed by using a classical optimization method [10], genetic algorithms [12], or any one proposed in [26].

This sub-process is illustrated in Fig. 3(a) for the example of the first-order bandpass filter (Fig. 1 with one dielectric post). Fig. 3(a) shows the starting 2D response (dashed line) for the initial 2D parameters $\mathbf{x}_{2D} = [l_c \ \phi]^T = [36.2 \ 6.86]^T$ mm and the optimized 2D response (dotted line) obtained for the specified discrete design specifications (f_{2D} , B_{2D}) = (4, 0.16) GHz. The optimization was implemented from a gradient-based optimization method. The number of 2D evaluations was 4. The optimal 2D parameters extracted from the optimized 2D response were $\mathbf{X}_{2D} = [l_c \ \phi]^T = [37 \ 11.4]^T$ mm.

B. Inverse Linear Input Space Mapping

The inverse linear input space-mapping optimization is reached by using a linear iterated prediction 2D to 3D* space mapping optimization procedure, which allows to find an approximate root of the system of nonlinear equations

$$\mathbf{X}_{3D,i+1}^* = \mathbf{P}^i(\mathbf{X}_{2D}) \quad i = 0, 1, 2, \dots \quad (2)$$

such that

$$\|\mathbf{e}\|_2^2 = \left(\sqrt{\sum_{i=1}^q |\mathbf{e}_i^T|^2} \right)^2 \leq \varepsilon \quad (3)$$

where \mathbf{X}_{2D} is the optimal 2D design parameter vector (1) and $\mathbf{X}_{3D,i+1}^*$ is the predicted 3D* design parameter vector at the ($i+1$)th iteration. ε is the error, $\|\mathbf{e}\|_2^2$ is the square of the Euclidean norm of the error vector $\mathbf{e} = [\mathbf{e}_1^T \dots \mathbf{e}_q^T]$, q is the number of discrete frequency points aligning the discrete design specifications of the 2D and 3D simulator responses (S -parameters), and \mathbf{e}_q is the q th error vector given by

$$\mathbf{e}_q = \mathbf{R}_{2D}(\mathbf{X}_{2D}, f_q) - \mathbf{R}_{3D}(\mathbf{X}_{3D,i+1}^*, \mathbf{X}_{3D,z}, f_q). \quad (4)$$

The multidimensional inverse linear mapping vector function \mathbf{P}^i (2) is iteratively estimated in two steps. The first step realizes an alignment of the \mathbf{R}_{2D} response with the discrete design specifications (center frequency, bandwidth) of the \mathbf{R}_{3D} response at the i th iteration. This step is aimed at extracting the 2D design parameter vector $\mathbf{X}_{2D,i}$ from the 3D* design parameter vector $\mathbf{X}_{3D,i}^*$

$$\mathbf{X}_{2D,i} = \arg \min_{\mathbf{x}_{2D}} \|\boldsymbol{\varepsilon}_1 \dots \boldsymbol{\varepsilon}_q\|_2^2. \quad (5)$$

The q th 2D design parameter extraction error vector is given by

$$\boldsymbol{\varepsilon}_q(\mathbf{x}_{2D}) = \mathbf{R}_{2D}(\mathbf{x}_{2D}, f_q) - \mathbf{R}_{3D}(\mathbf{X}_{3D,i}^*, \mathbf{X}_{3D,z}, f_q). \quad (6)$$

The second step establishes the inverse linear mapping between the 3D* and 2D design parameter vectors

$$\mathbf{X}_{3D,i}^* = \mathbf{P}^i(\mathbf{X}_{2D,i}) = \mathbf{A}^i + \mathbf{B}^i \mathbf{X}_{2D,i} \quad (7)$$

where \mathbf{A}^i and \mathbf{B}^i are the coefficient vectors calculated with the iterative procedure described in [28].

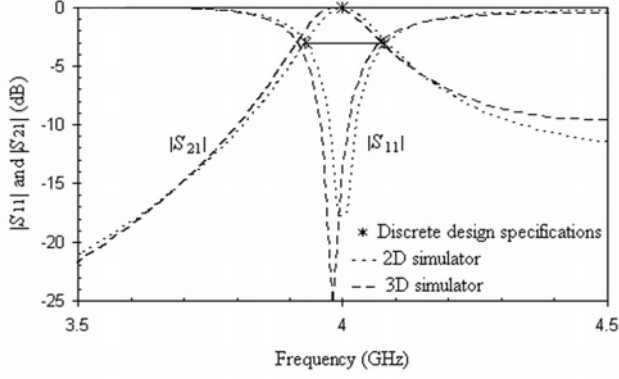


Fig. 4. First-order evanescent rectangular waveguide bandpass filter with one dielectric post: 2D and 3D simulator responses (S -parameters) for the optimal 2D and 3D design parameters obtained from the linear iterated prediction 2D to 3D space mapping procedure (second sub-process).

Fig. 3(b) illustrates the linear iterated prediction sub-process for the example with the first-order bandpass filter with one dielectric post (Fig. 1) and for one parameter: the diameter of the post. After four iterations (Fig. 3(b)) and an user-predefined error criterion $\varepsilon \leq 0.01$ (3), the optimized 3D parameter vector for our example was $\mathbf{X}_{3D}^* = [l_{c,3}^* \ \phi_3^*]^T = [40.3 \ 24.2]^T$ mm. In Fig. 4, it can be seen that the \mathbf{R}_{3D} response for this optimized vector presents a misalignment of 0.02 GHz with respect to the target \mathbf{R}_{2D} response. To further reduce this error, one has the option to increase the number of iterations, but this is time consuming, since each new iteration requires an additional 3D evaluation. To avoid this problem, a MANFIS is connected at the output, as shown in Fig. 2.

C. Output Neuro-Fuzzy Mapping Model

In our optimization procedure (Fig. 2), we use an output neuro-fuzzy mapping modeling process, which allows to reduce the residual error between \mathbf{R}_{2D} and \mathbf{R}_{3D} responses for the optimized parameters obtained from the above linear iterated prediction 2D to 3D* space mapping optimization procedure. The output neuro-fuzzy mapping modeling process is based on a multiple adaptive neuro-fuzzy inference system (MANFIS) [30], [31]. MANFIS is an extension of ANFIS to produce multiple real responses of the target system. The ANFIS is a fuzzy inference system implemented in the framework of an adaptive fuzzy neural network. The fuzzy inference system is a popular computing framework based on the concepts of fuzzy set theory, fuzzy if-then rules, and fuzzy reasoning. Among many fuzzy inference system models, we have used the Takagi and Sugeno's type [32], which is the most widely applied due to the accuracy, efficiency and high interpretability of its models.

The formulation of our optimization procedure (Fig. 2) with MANFIS is as follows. Assume that the vectors \mathbf{I} and \mathbf{O} represent the input and the output of MANFIS, respectively. Vector \mathbf{I} , common to a number d of ANFIS, is of size $l = (s + k + 1)$. The input parameters include the discrete design specifications (e.g., $s = \text{resonant frequency} + 3dB$

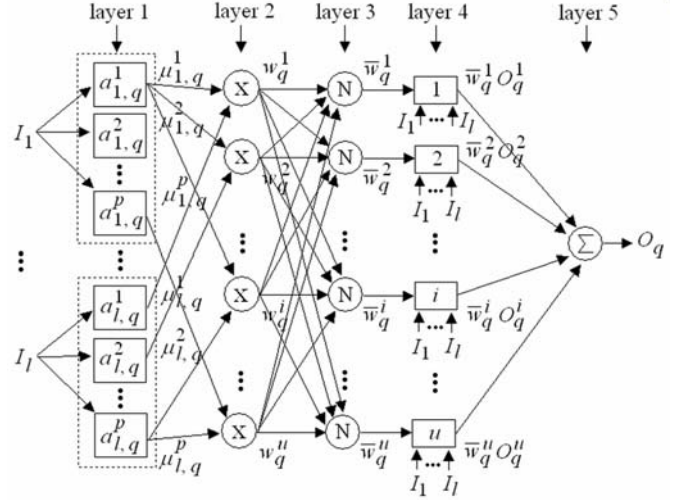


Fig. 5. Architecture of the q th adaptive neuro-fuzzy inference system (ANFIS) with l inputs and one output O_q .

bandwidth) extracted from the successive \mathbf{R}_{2D} responses to recover the \mathbf{R}_{3D} responses (second sub-process), the k design parameters of the third dimension $\mathbf{X}_{3D,z}$, and the discrete frequencies (f). Vector \mathbf{O} has a number $d = (n + s)$ of variables such as the n design parameters of \mathbf{X}_{3D} of the mapping \mathbf{P} , and the discrete design specifications (s) extracted from the successive \mathbf{R}_{3D} responses. The number of ANFIS is equal to the number d of output variables. The architecture of the q th ANFIS with l inputs (I_1, \dots, I_l) and one output (O_q) is shown in Fig. 5. It consists of five layers, two of them having adjustable weights (represented by square boxes). In this q th ANFIS, the rule base would contain a number u of fuzzy if-then rules of Takagi and Sugeno's type [32]

$$\begin{aligned}
 R_q^1 &: \text{If } I_1 \text{ is } a_{1,q}^1 \dots \text{ and } I_l \text{ is } a_{l,q}^1, \text{ then } O_q^1 = r_{1,q}^1 I_1 + \dots + r_{l,q}^1 I_l + r_{0,q}^1 \\
 R_q^2 &: \text{If } I_1 \text{ is } a_{1,q}^2 \dots \text{ and } I_l \text{ is } a_{l,q}^2, \text{ then } O_q^2 = r_{1,q}^2 I_1 + \dots + r_{l,q}^2 I_l + r_{0,q}^2 \\
 &\dots \\
 R_q^i &: \text{If } I_1 \text{ is } a_{1,q}^i \dots \text{ and } I_l \text{ is } a_{l,q}^i, \text{ then } O_q^i = r_{1,q}^i I_1 + \dots + r_{l,q}^i I_l + r_{0,q}^i \\
 &\dots \\
 R_q^u &: \text{If } I_1 \text{ is } a_{1,q}^u \dots \text{ and } I_l \text{ is } a_{l,q}^u, \text{ then } O_q^u = r_{1,q}^u I_1 + \dots + r_{l,q}^u I_l + r_{0,q}^u
 \end{aligned} \tag{8}$$

where R_q^i ($i = 1, \dots, u$ and $q = 1, 2, \dots, d$) denotes the i th fuzzy rule of the q th adaptive neuro-fuzzy inference system. I_j ($j = 1, \dots, l$) is the j th component of vector \mathbf{I} . O_q^i is the real output of the fuzzy rule R_q^i . $a_{j,q}^h$ ($h = 1, \dots, p$) are the linguistic labels (small, large, etc.), which are assigned to a corresponding membership function. Among different membership functions, we have used Gaussian membership function. If the number of linguistic labels (membership functions) associated to each input is h , then the number u of fuzzy rules, common to each adaptive neuro-fuzzy inference

system, is equal to $u = p^l$. Finally, $r_{j,q}^i$ are parameters called consequent parameters.

The first layer (Fig. 5) implements a number $l \times u$ of fuzzy decision rules by means of p membership functions, like for example

$$\mu_{j,q}^h(I_j) = \exp \left[\frac{-1}{2} \left(\frac{I_j - b_{j,q}^h}{\sigma_{j,q}^h} \right)^2 \right] \quad (9)$$

where $\mu_{j,q}^h(I_j)$ ($h=1, \dots, p$) is the membership function of $a_{j,q}^h$ associated to the input I_j . It specifies the degree to which the given I_j satisfies the quantifier $a_{j,q}^h$. Also, $(b_{j,q}^h, \sigma_{j,q}^h)$ is the parameter set that changes the shapes of the Gaussian membership function. These parameters are referred as the premise parameters.

The second layer computes every possible conjunction of the $l \times u$ decision rules via multiplication

$$\begin{aligned} w_q^1 &= \mu_{1,q}^1(I_1) \times \mu_{2,q}^1(I_2) \times \dots \times \mu_{l,q}^1(I_l) \\ w_q^2 &= \mu_{1,q}^2(I_1) \times \mu_{2,q}^2(I_2) \times \dots \times \mu_{l,q}^2(I_l) \\ &\dots \\ w_q^i &= \mu_{1,q}^i(I_1) \times \mu_{2,q}^i(I_2) \times \dots \times \mu_{l,q}^i(I_l) \\ &\dots \\ w_q^u &= \mu_{1,q}^u(I_1) \times \mu_{2,q}^u(I_2) \times \dots \times \mu_{l,q}^u(I_l) \end{aligned} \quad (10)$$

The third layer normalizes the conjunctives membership functions in order to rescale the inputs

$$\bar{w}_q^i = w_q^i / \sum_{i=1}^u w_q^i. \quad (11)$$

In the fourth layer, each node associates every normalized membership function with an output

$$\bar{w}_q^i \times O_q^i = \bar{w}_q^i (r_{1,q}^i I_1 + \dots + r_{l,q}^i I_l + r_{0,q}^i). \quad (12)$$

Finally, the fifth layer sums the two outputs of the previous layer

$$O_q = \sum_{i=1}^u \bar{w}_q^i \times O_q^i = \sum_{i=1}^u w_q^i O_q^i / \sum_{i=1}^u w_q^i. \quad (13)$$

O_q is the q th component of the vector \mathbf{O} and it corresponds to the output of the q th adaptive neuro-fuzzy inference system. The output O_q is a real number. During the learning process, the premise parameters in layer 1 and the consequent

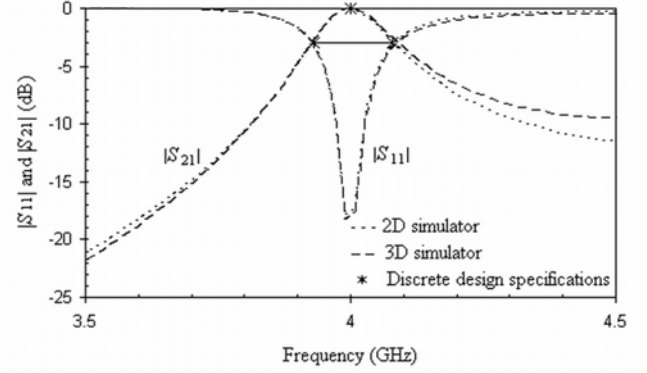


Fig. 6. First-order evanescent rectangular waveguide bandpass filter with one dielectric post: 2D and 3D simulator responses (S -parameters) for the optimal 2D and 3D design parameters (third sub-process).

parameters in layer 4 are tuned until the desired output response of the adaptive neuro-fuzzy inference system is obtained. In this paper, a hybrid learning algorithm [30] combining the least square method and the gradient descent method is used to fast train the adaptive neuro-fuzzy inference system.

For the application of this neuro-fuzzy technique to the example of the first-order bandpass filter (Fig. 1 with one dielectric post), the successive discrete design specifications extracted from \mathbf{R}_{2D} and \mathbf{R}_{3D} , and the successive design parameters $\mathbf{X}_{3D,i}^*$ obtained at the different iterations of the linear iterated prediction algorithm, are included in the corresponding input \mathbf{I} and output \mathbf{O} vectors. Thus, the input parameters are the center frequency of \mathbf{R}_{2D} (f_{2D}), the 3 dB bandwidth of \mathbf{R}_{2D} (B_{2D}), the discrete frequencies and the fixed height of the post at the different iterations: $\mathbf{I} = [f_{2D} B_{2D} f h_1]^T$. The output parameters are the optimized length of the evanescent waveguide section (l_c^*), the optimized diameter of the post (ϕ^*), the center frequency of \mathbf{R}_{3D} (f_{3D}), and the 3 dB bandwidth of the \mathbf{R}_{3D} (B_{3D}) at the different iterations: $\mathbf{O} = [l_c^* \phi^* f_{3D} B_{3D}]^T$. The number of ANFIS is, therefore, four. During the training phase, the total number of data was 404 (101 frequency points \times 4 iterations). Half of data (202) were used for training and the other half for testing. Three epochs were sufficient to train each ANFIS with 16 fuzzy rules. Additional parameters are 2 Gaussian membership functions per input, 16 and 96 premise and consequent parameters per adaptive neuro-fuzzy inference system, respectively. The maximum relative error over expected \mathbf{X}_{3D}^M and \mathbf{R}_{3D}^M (discrete 3D design specifications) test data was lower than $6.4 \cdot 10^{-4} \%$ for this structure.

Once the training of the MANFIS is completed, we have available a nonlinear output space mapping model. Fig. 3(c) shows the output neuro-fuzzy mapping for the diameter of the post. Thus, the optimal 3D* design parameters \mathbf{X}_{3D}^M of the corresponding filter are accurately computed from this sub-

process. $\mathbf{X}_{3D^*}^M$ is obtained by applying, in the MANFIS input, the initial vector with the discrete 2D design specifications to be achieved: $\mathbf{I}_{in} = [f_{2D} \ B_{2D} \ f \ h_1]^T = [4 \ 0.16 \ f \ 18.05]^T$. The optimal 3D* design parameter vector was $\mathbf{X}_{3D^*}^M = [39.95 \ 24.04]^T$ mm, which is slightly different to the previous $\mathbf{X}_{3D}^* = [40.3 \ 24.2]^T$ mm. Fig. 6 shows the 2D and 3D simulator responses with the optimal 2D (\mathbf{X}_{2D}) and 3D ($\mathbf{X}_{3D^*}^M$) design parameters. It can be seen that the 3D simulator response is in good agreement with the initial discrete design specifications. Due to the use of MANFIS, the ε error (3) is lower than 1.5×10^{-3} . This represents an improvement in accuracy of 85% with respect to the user-predefined error ($\varepsilon = 0.01$) achieved during the inverse linear input space-mapping optimization. In the next sub-section, we summarize the whole optimization procedure in twelve different simple steps.

D. Implementation details

A summary of the proposed implementation can be described from the following steps:

1. Set $i=0$, optimize \mathbf{R}_{2D} to find (1) and obtain the initial vector \mathbf{I}_{in} ;
2. Obtain \mathbf{R}_{3D} at $\mathbf{X}_{3D,0}^* = \mathbf{X}_{2D}$ and \mathbf{O}_0 ;
3. Optimize \mathbf{R}_{2D} to find (5) and obtain \mathbf{I}_0 ;
4. Find the coefficients of (7) and compute $\mathbf{X}_{3D,1}^*$ from (2);
5. Obtain \mathbf{R}_{3D} at $\mathbf{X}_{3D,1}^*$ and \mathbf{O}_1 ;
6. Set $i=i+1$, optimize \mathbf{R}_{2D} to find (5) and \mathbf{I}_i ;
7. Find the coefficients of (7) and compute $\mathbf{X}_{3D,i+1}^*$ from (2);
8. Obtain \mathbf{R}_{3D} at $\mathbf{X}_{3D,i+1}^*$ and \mathbf{O}_{i+1} ;
9. Optimize \mathbf{R}_{2D} to find (5) and obtain \mathbf{I}_{i+1} ;
10. Compare \mathbf{R}_{2D} of Step 1 with \mathbf{R}_{3D} of Step 8. If the execution condition (3) is not satisfied and the user-defined number of iterations is not exceeded go to step 6.
11. Prepare and train the MANFIS with \mathbf{I} and \mathbf{O} ;
12. Compute $\mathbf{X}_{3D^*}^M$ and \mathbf{R}_{3D}^M with MANFIS at \mathbf{I}_{in} ; END.

III. APPLICATION TO THE OPTIMIZATION-ORIENTED DESIGN OF HIGHER ORDER EVANESCENT RECTANGULAR WAVEGUIDE BANDPASS FILTERS

To demonstrate the usefulness of the proposed technique for the optimization-oriented design of practical narrow bandpass microwave filters, we have applied the same technique to the design of higher order bandpass filters based on 3D evanescent rectangular waveguides with dielectric posts (Fig. 1). As application examples, we have considered a

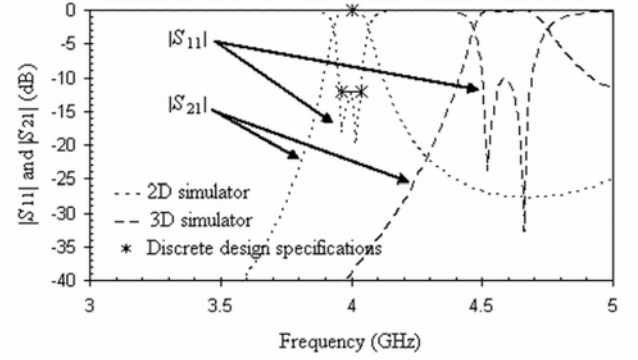


Fig. 7. Magnitude of S_{11} and S_{21} for the second-order evanescent rectangular waveguide bandpass filter with two dielectric posts before 2D to 3D space mapping optimization ($h_1 = 18.05$ mm).

second-order and sixth-order bandpass filters. The input/output waveguides are of standard WR-229 type with dimensions $(a, b) = (58.1, 29.05)$ mm. The fixed design parameters are: $\varepsilon_r = 4$, $h_1 = 18.05$ mm ($h_2 = 5.5$ mm), $c = 31.1$ mm and $c = 32.1$ mm for the second-order and sixth-order filters, respectively. The posts are centered in the evanescent waveguide section of length l_c . The simulations were realized on an Intel Pentium 4 (3-GHz CPU) computer with 1-GB RAM for 101 frequency points and $3 \text{ GHz} \leq f \leq 5 \text{ GHz}$.

According to Fig. 1 and the ILINFO-SM technique (Fig. 2), the 2D parameter space of the second-order filter is composed of $\mathbf{x}_{2D} = [l_c \ \phi_1 \ \phi_2 \ d_{c_1}]^T$, where d_{c_1} is the distance between the centers of the two dielectric posts. A symmetrical filter was considered: $\phi_2 = \phi_1$. The 3D parameter space is $\mathbf{x}_{3D}^* = [l_c^* \ \phi_1^* \ \phi_2^* \ d_{c_1}^*]^T$, together with the third dimension, which is the height of the posts fixed to $h_1 = X_{3D,z} = 18.05$ mm. The initial discrete 2D design specifications to be achieved for this filter are the center frequency $f_{2D} = 4$ GHz and the equal-ripple bandwidth $B_{2D} = 0.1$ GHz.

In the first step of the algorithm (Section II D), the initial vector according to predefined discrete 2D design specifications was: $\mathbf{I}_{in} = [f_{2D} \ B_{2D} \ f \ h_1]^T = [4 \ 0.1 \ f \ 18.05]^T$. The optimal 2D design parameters (Step 1) verifying the above initial discrete design specifications were $\mathbf{X}_{2D} = [l_c \ \phi_1 \ \phi_2 \ d_{c_1}]^T = [92 \ 11.4 \ 11.4 \ 55]^T$ mm. They constitute the target responses of the ILINFO-SM approach. At these optimal 2D design parameters ($\mathbf{x}_{3D}^* = \mathbf{X}_{2D}$), the responses of the 2D and 3D simulators are as in Fig. 7. A disagreement is observed before 2D to 3D optimization.

Following the successive steps until Step 10 of the optimization procedure described in Section II D, we obtain the design parameters \mathbf{X}_{3D}^* for this second-order bandpass filter. For an error condition (3) set to $\varepsilon \leq 0.01$, the solution of this filter was achieved with four 3D simulator evaluations. The design parameters \mathbf{X}_{3D}^* obtained with the iterated

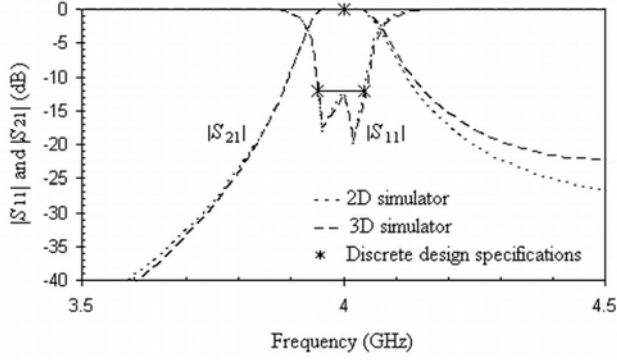


Fig. 8. Second-order evanescent rectangular waveguide bandpass filter with two dielectric posts: 2D and 3D simulator responses (S -parameters) for the optimal 2D and 3D design parameters ($h_1 = 18.05$ mm).

prediction procedure were $\mathbf{X}_{3D}^* = [98.2 \ 24.6 \ 24.6 \ 58.3]^T$ mm. In the meantime, the successive discrete design specifications extracted from \mathbf{R}_{2D} and \mathbf{R}_{3D} , and the successive design parameters $3D^*$, were included in the corresponding input $\mathbf{I} = [f_{2D} \ B_{2D} \ f \ h_1]^T$ and output $\mathbf{O} = [I_c^* \ \phi_1^* \ \phi_2^* \ d_{c_1}^* \ f_{3D} \ B_{3D}]^T$ vectors.

In the next Step 11, we prepare five ANFIS ($\phi_2^* = \phi_1^*$) and train them with the input \mathbf{I} and output \mathbf{O} vectors. During the training phase, the total number of data was 404 (101 frequency points \times 4 iterations). Half of data (202) were used for training and the other half for testing. Three epochs were sufficient to train each ANFIS with 16 fuzzy rules. Additional parameters are 2 Gaussian membership functions per input, 16 and 96 premise and consequent parameters per ANFIS, respectively. The maximum relative error over expected \mathbf{X}_{3D}^M and \mathbf{R}_{3D}^M (discrete 3D design specifications) test data was lower than $3 \times 10^{-3} \%$ for this filter.

Finally, the optimal $3D^*$ design parameters \mathbf{X}_{3D}^M of the corresponding filter are accurately computed in Step 12 by applying, in the MANFIS input, the vector $\mathbf{I}_{in} = [4 \ 0.1 \ f \ 18.05]^T$. The results obtained were $\mathbf{X}_{3D}^M = [97.98 \ 23.9 \ 23.9 \ 58.25]^T$ mm, which are slightly different to the previous $\mathbf{X}_{3D}^* = [98.2 \ 24.6 \ 24.6 \ 58.3]^T$ mm (Step 10). Fig. 8 shows the 2D and 3D simulator responses corresponding to the second-order bandpass filter with the optimal 2D (\mathbf{X}_{2D}) and 3D* (\mathbf{X}_{3D}^M) design parameters, for a height of the posts fixed to $h_1 = 18.05$ mm. It can be seen that the 3D simulator response of the 3D structure is in good agreement with the initial discrete design specifications. Due to the use of MANFIS, the ε error (3) is lower than 1.8×10^{-3} . This represents an improvement in accuracy of 82% with respect to the user-predefined error ($\varepsilon = 0.01$) achieved during the inverse linear input space-mapping optimization.

In order to assess the computational cost of the approach when the complexity of the structure increases, Table I shows

TABLE I
ILINFO-SM OPTIMIZATION RESULTS FOR THE FIRST-ORDER AND SECOND-ORDER EVANESCENT RECTANGULAR WAVEGUIDE BANDPASS FILTERS

Details	First-order filter	Second-order filter
N° of 2D evaluations	17	17
N° of 3D evaluations	4	4
Total 2D evaluation time	15.18 min (3.44 %)	38.15 min (6.91 %)
Total 3D evaluation time	7 h 05.39min (96.55 %)	8 h 42.03min (93.18 %)
Total MANFIS training, test and evaluation time	2 s (0.01 %)	3 s (0.01 %)
Total optimization time	7 h 20.59 min	9 h 20.21 min

TABLE II
OPTIMIZATION RESULTS FOR THE SECOND-ORDER EVANESCENT RECTANGULAR WAVEGUIDE BANDPASS FILTER

Details	Our approach	EM-MANFIS method
N° of 2D simulator evaluations	17	—
N° of 3D simulator evaluations	4	14
Total 2D evaluation time	38.15 min	—
Total 3D evaluation time	8 h 42.03 min	24 h 08.56 min
Total MANFIS training, test and evaluation time	3 s	15 s
Total optimization time	9 h 20.21 min	24 h 09.11 min

the useful optimization data obtained from our ILINFO-SM approach for the first-order and second-order evanescent rectangular waveguide bandpass filters. The number of the parameters to be optimized is 2 and 3 for the first-order bandpass filter and second-order bandpass filter, respectively. Due to the need to optimize an additional parameter in the case of the second-order bandpass filter, the computational cost has approximately increased in 151%, 22% and 30% for the total 2D evaluation time, total 3D evaluation time and total optimization time, respectively. Although the total 2D evaluation time has increased considerably adding one parameter to the structure, it can be seen in Table I that its computational cost represents less than 7% of the total optimization time. In table I, we can see the importance to reduce the number of 3D analysis to avoid very large computational times, since it represents more than 90% of the total cost. With the proposed technique, the whole structure can be optimized with only four 3D evaluations.

In order to compare our approach with other techniques, we include in Table II details of the optimization results for the second-order evanescent rectangular waveguide bandpass filter with two dielectric posts obtained from an electromagnetic-multiple adaptive neuro-fuzzy inference system (EM-MANFIS) method similar to [16], [17], and from our proposed approach. For the test, we have substituted the artificial neural network in [16], [17] by MANFIS. To produce a similar accuracy to our approach ($\varepsilon = 1.8 \times 10^{-3}$), fourteen 3D simulator evaluations randomly distributed in the region of interest were needed to create the EM-MANFIS model. The region of interest was obtained from the previous optimization process with our proposed approach: $90 \text{ mm} \leq$

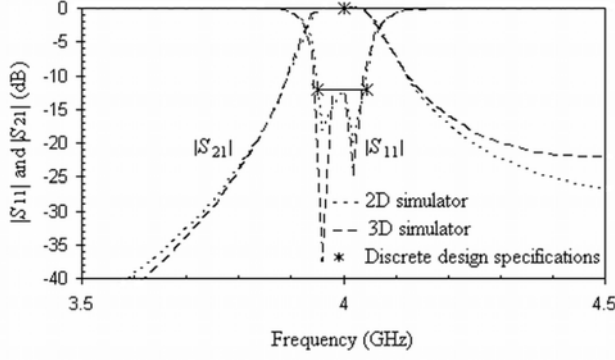


Fig. 9 Interpolation results for the second-order evanescent rectangular waveguide bandpass filter with two dielectric posts: 2D and 3D simulator responses (S -parameters) for the optimal 2D and 3D design parameters ($h_1 = 17.5$ mm).

$l_c^* \leq 100$ mm, 5.5 mm $\leq \phi_1^* \leq 13$ mm, 55 mm $\leq d_{c_1}^* \leq 60$ mm and $\phi_2^* = \phi_1^*$. If the region of interest is not previously known, even more 3D evaluations would be required to create the model with similar accuracy. Although our approach has required seventeen 2D simulator evaluations, the total optimization time is larger for the EM-MANFIS method, due to the higher number of evaluations in the time consuming 3D space.

Up to now MANFIS has been used to reduce the error of the iterated linear prediction algorithm, without the need to increase the number of time consuming 3D simulations. However, the interpolation capabilities of MANFIS can be further exploited to optimize the design process of the filters if different heights of the dielectric posts need to be considered in a practical situation. To show the performance of MANFIS in this task, in a first step we have optimized this second-order bandpass filter with the same above structure and initial discrete design specifications, but with a different height of the posts ($h_1 = 17.05$ mm). At $h_1 = 17.05$ mm, the design parameters X_{3D}^* obtained with the iterated prediction procedure were $X_{3D}^* = [98.80 \ 26.36 \ 24.36 \ 58.67]^T$ mm. The data of the successive iterations were introduced at the previous I and O vectors, together with data generated for the previous height: $h_1 = 18.05$ mm. In a second step, we have trained MANFIS with 3 epochs. Once MANFIS is trained, it can directly be used, without the need of further optimizations, to obtain the design of a filter when the dielectric posts have a different height. For instance, we have extracted the optimal 3D* design parameters for an intermediate height of the posts: $h_1 = 17.5$ mm. The optimal 3D* design parameters were $X_{3D}^M = [99.87 \ 25.38 \ 25.38 \ 58.91]^T$ mm for $I_{in} = [f_{2D} \ B_{2D} \ f \ h_1]^T = [4 \ 0.1 \ f \ 17.5]^T$. As it can be seen in Fig. 9, the optimal solution X_{3D}^M for $h_1 = 17.5$ mm, satisfies the initial discrete design specifications in a very accurate way, and without any extra optimization procedure.

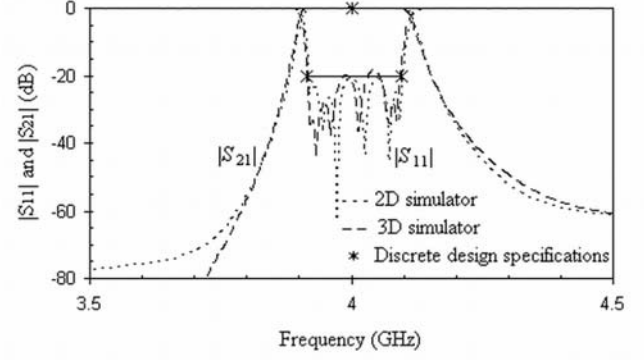


Fig. 10 Sixth-order evanescent rectangular waveguide bandpass filter with six dielectric posts: 2D and 3D simulator responses (S -parameters) for the optimal 2D and 3D design parameters ($h_1 = 18.05$ mm).

Finally, by applying the proposed technique to several second-order structures, the coupling coefficients of higher order filters can be efficiently obtained for the design of more complex microwave filters [7]. To illustrate the procedure we have selected a sixth-order bandpass filter. The initial discrete 2D design specifications to be achieved for this filter are the center frequency $f_{2D} = 4$ GHz and the equal-ripple bandwidth $B_{2D} = 0.18$ GHz (relative bandwidth of 4.5 %). All other fixed dimensions shown in Fig. 1 are the same as above except for $c = 32.1$ mm. A symmetrical filter was considered: $\phi_4 = \phi_3$, $\phi_5 = \phi_2$, $\phi_6 = \phi_1$, $d_{c_4} = d_{c_2}$ and $d_{c_5} = d_{c_1}$. Using well known synthesis techniques [35], the coupling matrix of the filter to be designed was:

$$M = \begin{bmatrix} 0 & 1.082 & 0 & 0 & 0 & 0 & 0 \\ 1.082 & 0 & 0.843 & 0 & 0 & 0 & 0 \\ 0 & 0.843 & 0 & 0.611 & 0 & 0 & 0 \\ 0 & 0 & 0.611 & 0 & 0.583 & 0 & 0 \\ 0 & 0 & 0 & 0.583 & 0 & 0.611 & 0 \\ 0 & 0 & 0 & 0 & 0.611 & 0 & 0.843 \\ 0 & 0 & 0 & 0 & 0 & 0.843 & 1.082 \\ 0 & 0 & 0 & 0 & 0 & 0 & 1.082 \end{bmatrix} \quad (14)$$

The source/load coupling to the first/last resonator ($M_{S1} = M_{6L} = 1.002$) is adjusted by applying our optimization technique to a doubly terminated single resonator, as explained in Section II. This optimization has required 4 evaluations of the 3D EM simulator. All other inter-resonator couplings are extracted by applying our optimization technique to a structure composed of two coupled resonators, maintaining the input/output coupling obtained in the previous step. A total of 12 evaluations of the 3D simulator were needed for the optimization of the three remaining couplings ($M_{12} = M_{56} = 0.843$, $M_{23} = M_{45} = 0.611$ and $M_{34} = 0.583$). The optimal 2D and 3D design parameters for the sixth-order bandpass filter were $X_{2D} = [l_c \ \phi_1 \ \phi_2 \ \phi_3 \ d_{c_1}$

$d_{c_2} \ d_{c_3}]^T = [288.6 \ 10.78 \ 10.76 \ 10.76 \ 49.2 \ 55.4 \ 56.4]^T$ mm and $X_{3D}^M = [304.65 \ 21.38 \ 21.3 \ 21.28 \ 51.82 \ 58.1 \ 59.19]^T$ mm, respectively. Fig. 10 shows the optimized 2D and 3D responses at the final solution. Both responses exhibit a very good agreement inside the passband of the filter.

IV. CONCLUSION

A technique for the optimization-oriented design of 3D radiofrequency and microwave circuits has been presented. This technique reduces the number of analysis needed with time consuming 3D electromagnetic simulators, by performing optimization with fast 2D electromagnetic simulators, and a proper mapping between the 2D and 3D spaces. The mapping is obtained from an inverse-linear-input space-mapping approach and a neuro-fuzzy-output space-mapping technique using a multiple adaptive neuro-fuzzy inference system (MANFIS). The neuro-fuzzy output reduces the residual error, and facilitates further optimizations and interpolations, which can not be carried out with an inverse linear input mapping. Our inverse-linear-input neuro-fuzzy-output space-mapped (ILINFO-SM) technique has been successfully applied to the optimization and interpolation of first-order, second-order and sixth-order C-band 3D evanescent rectangular waveguide bandpass filters with dielectric posts.

REFERENCES

- [1] T. Itoh, Ed., *Numerical techniques for microwave and millimeter-wave passive structures*. John Wiley & Sons, 1989.
- [2] A. F. Peterson, S. L. Ray, and R. Mittra, *Computational methods for electromagnetics*. Piscataway, NJ: IEEE Press, 1998.
- [3] F. D. Quesada Pereira, V. E. Boria Esbert, J. Pascual Garcia, A. Vidal Pantaleoni, A. Alvarez Melcon, J. L. Gomez Tornero, and B. Gimeno, "Efficient analysis of arbitrary shaped inductive obstacles in rectangular waveguides using a surface integral equation formulation," *IEEE Trans. Microw. Theory Tech.*, vol. 55, no. 4, pp. 715-721, Apr. 2007.
- [4] R. C. Booton, "Microwave CAD in the year 2010 - A panel discussion," *Int. J. of RF and Microw. CAE*, vol. 9, no. 6, pp. 439-447, Oct. 1999.
- [5] M. B. Steer, J. W. Bandler, and C. M. Snowden, "Computer-aided design of RF and microwave circuits and systems," *IEEE Trans. Microw. Theory Tech.*, vol. 50, no. 3, pp. 996-1005, Mar. 2002.
- [6] F. Arndt, J. Brandt, V. Catina, J. Ritter, I. Rullhusen, J. Dauelsberg, U. Hilgert, and W. Wessel, "Fast CAD and optimization of waveguide components and aperture antennas by hybrid MM/FE/MoM/FD methods - State-of-the-art and recent advances," *IEEE Trans. Microw. Theory Tech.*, vol. 52, no. 1, pp. 292-305, Jan. 2004.
- [7] R. Levy, R. V. Snyder, and G. Matthaei, "Design of microwave filters," *IEEE Trans. Microw. Theory Tech.*, vol. 50, no. 3, pp. 783-793, Mar. 2002.
- [8] D. Swanson and G. Macchiarella, "Microwave filter design by synthesis and optimization," *IEEE Microw. Mag.*, vol. 8, no. 2, pp. 55-69, Apr. 2007.
- [9] S. W. Director, "Survey of circuit-oriented optimization techniques," *IEEE Trans. Circuits Theory*, vol. CT-18, no. 1, pp. 3-10, Jan. 1971.
- [10] S. Rosloniec, *Algorithms for computer-aided design of linear microwave circuit*. Boston, MA: Artech House, 1990.
- [11] J. W. Bandler and S. H. Chen, "Circuit optimization: The state of the art," *IEEE Trans. Microw. Theory Tech.*, vol. 36, no. 2, pp. 424-443, Feb. 1998.
- [12] Y. Rahmat-Samii and E. Michielssen, *Electromagnetic optimization by genetic algorithms*. New York, NY: John Wiley & Sons, 1999.
- [13] N. Damavandi and S. Safadi-Naeini, "A hybrid evolutionary programming method for circuit optimization," *IEEE Trans. Circuits Syst. I, Reg. Papers*, vol. 52, no. 5, pp. 902-910, May 2005.
- [14] J. W. Bandler and M. Mongiardo, Eds., "Special Issue on Electromagnetics-based optimization of microwave components and circuits," *IEEE Trans. Microw. Theory Tech.*, vol. 52, no. 1, pp. 245-456, Jan. 2004.
- [15] T. Laxminidhi, and S. Pavan, "Efficient design centering of high-frequency integrated continuous-time filters," *IEEE Trans. Circuits Syst. I, Reg. Papers*, vol. 54, no. 7, pp. 1481-1488, July 2007.
- [16] A. H. Zaabab, Q. J. Zhang, and M. S. Nakhla, "Analysis and optimization of microwave circuits and devices using neural network models," in *Proc. IEEE MTT-S Int. Microwave Symp. Dig.*, San Diego, CA, May 1994, pp. 393-396.
- [17] P. Burrascano, M. Dionigi, C. Fancelli, and M. Mongiardo, "A neural network model for CAD and optimization of microwave filters," in *Proc. IEEE MTT-S Int. Microwave Symp. Dig.*, Baltimore, MD, Jun. 1998, pp. 13-16.
- [18] T. Kim, X. Li, and D. J. Allstot, "Compact model generation for on-chip transmission lines," *IEEE Trans. Circuits Syst. I, Reg. Papers*, vol. 51, no. 3, pp. 459-470, March 2004.
- [19] V. Miraftab and R. R. Mansour, "Computer-aided tuning of microwave filters using fuzzy logic," *IEEE Trans. Microw. Theory Tech.*, vol. 50, no. 12, pp. 1605-1608, Dec. 2002.
- [20] E. B. Rahouyi, J. Hinojosa, and J. Garrigos, "Neuro-fuzzy modeling techniques for microwave components," *IEEE Microw. Wireless Compon. Lett.*, vol. 16, no. 2, pp. 72-74, Feb. 2006.
- [21] V. Miraftab and R. R. Mansour, "Fully automated RF/microwave filter tuning by extraction human experience using fully controllers," *IEEE Trans. Circuits Syst. I, Reg. Papers*, vol. 55, no. 5, pp. 1357-1367, Jun. 2008.
- [22] J. W. Bandler, M. A. Ismail, J. E. Rayas-Sánchez, and Q.-J. Zhang, "Neuromodeling of microwave circuits exploiting space-mapping technology," *IEEE Trans. Microw. Theory Tech.*, vol. 47, no. 12, pp. 2417-2427, Dec. 1999.
- [23] J. Hinojosa and G. Doménech-Asensi, "Space-mapped neuro-fuzzy optimization for microwave device modeling," *Microw. and Opt. Technology Lett.*, vol. 49, no. 6, pp. 1328-1334, Jun. 2007.
- [24] J. W. Bandler, R. M. Biernacki, and S. H. Chen, "Fully automated space mapping optimization of 3D structures," in *Proc. IEEE MTT-S Int. Microw. Symp. Dig.*, San Francisco, CA, Jun. 1996, pp. 753-756.
- [25] J. W. Bandler, R. M. Biernacki, S. H. Chen and D. Omeragic, "Space mapping optimization of waveguide filters using finite element and mode-matching electromagnetic simulators," in *Proc. IEEE MTT-S Int. Microw. Symp. Dig.*, Denver, CO, Jun. 1997, pp. 635-638.
- [26] J. W. Bandler, Q. S. Cheng, S. A. Dakroury, A. S. Mohamed, M. H. Bakr, K. Madsen, and J. Sondergaard, "Space mapping: The state of the art," *IEEE Trans. Microw. Theory Tech.*, vol. 52, no. 1, pp. 337-361, Jan. 2004.
- [27] J. E. Rayas-Sánchez and V. Gutiérrez-Ayala, "EM-based Monte Carlo analysis and yield prediction of microwave circuits using linear-input neural-output space mapping," *IEEE Trans. Microw. Theory Tech.*, vol. 54, no. 12, pp. 4528-4537, Dec. 2006.
- [28] J. Hinojosa, F. D. Quesada-Pereira, and A. Alvarez-Melcon, "2D to 3D rectangular waveguide filter designs from linear iterated prediction space mapping optimization," *Microw. and Opt. Technology Lett.*, vol. 51, no. 8, pp. 1979-1983, Aug. 2009.
- [29] J. Doynne Farmer and J. J. Sidorowich, "Predicting chaotic time series," *Phys. Rev. Lett.*, vol. 59, no. 8, pp. 845-848, Aug. 1987.
- [30] J.-S. R. Jang, "ANFIS: Adaptive-network-based fuzzy inference system," *IEEE Trans. Syst. Man. Cybern.*, vol. 23, no. 3, pp. 665-685, May/Jun. 1993.
- [31] J.-S. R. Jang, C.-T. Sun and E. Mizutami, *Neuro-fuzzy and soft computing: A computational approach to learning and machine intelligence*. Englewood Cliffs, NJ: Prentice Hall, 1997.
- [32] T. Takagi and M. Sugeno, "Fuzzy identification of systems and its applications to modeling and control," *IEEE Trans. Syst. Man. Cybern.*, vol. 15, no. 1, pp. 116-132, Jan./Feb. 1985.
- [33] R. R. Mansour, "Filter technology for wireless base stations," *IEEE Microw. Mag.*, vol. 5, no. 1, pp. 68-74, Mar. 2004.
- [34] V. E. Boria and B. Gimeno, "Waveguide filters for satellites," *IEEE Microw. Mag.*, vol. 8, no. 5, pp. 60-70, Oct. 2007.

- [35] R. J. Cameron, Chandra M. Kudsia and Raafat R. Mansour, *Microwave Filters for Communication Systems*. Hoboken, NJ: John Wiley & Sons, 2007, ch. 7.



Juan Hinojosa was born in Dunkerque, France, in 1965. He received the Diplôme d'Etudes Approfondies (DEA) and the Ph.D. degrees in electronics from the Université des Sciences et Technologies de Lille (USTL), Lille, France, in 1990 and 1995, respectively.

In 1990, he joined the Hyper-frequency and Semiconductor Department of the Nanotechnologies and Microelectronics, Electronics Institute (IEMN), USTL, as a Research Student, where he was involved in the development of electromagnetic

characterization techniques of materials at the microwave frequency range. In 1999, he joined the Universidad Politécnica de Cartagena, Cartagena, Spain, where he currently develops his teaching and research activities. His research interests include EM characterization techniques of materials at the microwave frequency range and microwave circuit and device modeling techniques for novel microwave passive circuit and device design.



Fernando D. Quesada Pereira (S'05-A'07) was born in Murcia, Spain, in 1974. He received the Telecommunications Engineer degree from the Technical University of Valencia (UPV), Valencia, Spain, in 2000, and the Ph.D. degree from the Technical University of Cartagena (UPCT),

Cartagena, Spain in 2007. In 1999, he joined the Radiocommunications Department, UPV, as a Research Assistant, where he was involved in the development of numerical methods for the analysis of anechoic chambers and tag antennas. In 2001, he joined the Communications and Information Technologies Department, UPCT, initially as a Research Assistant, and then as an Assistant Professor. In 2005, he spent six months as a Visiting Scientist with the University of Pavia, Pavia, Italy. In 2009, he was an invited researcher for five months at the Technival University of Valencia (iTeam), Spain. His current scientific interests include IE numerical methods for the analysis of antennas and microwave devices.



Monica Martinez Mendoza was born in Cartagena, Murcia, Spain, in 1983. She received the Telecommunications Engineer degree from the Technical University of Cartagena (UPCT), Spain, in 2006. In 2007 she joined the Telecommunication and Electromagnetic group, UPCT, as a research assistant, where she was involved in the development of novel transversal filtering structures for satellite systems. She is currently working towards the Ph.D. degree in the European Space

Agency (ESTEC, The Netherlands) together with the UPCT under the NPI Initiative. Her current scientific interests include the analysis and design of microwave circuits.



Alejandro Alvarez Melcón (M'99-SM'07) was born in Madrid, Spain, in 1965. He received the Telecommunications Engineer degree from the Technical University of Madrid (UPM), Madrid, Spain, in 1991, and the Ph.D. degree in electrical engineering from the Swiss Federal Institute of Technology, Lausanne, Switzerland, in 1998.

In 1988, he joined the Signal, Systems and Radiocommunications Department, UPM, as a research student, where he was involved in the design, testing, and measurement of broad-band

spiral antennas for electromagnetic measurements support (EMS) equipment.

From 1991 to 1993, he was with the Radio Frequency Systems Division, European Space Agency (ESA/ESTEC), Noordwijk, The Netherlands, where he was involved in the development of analytical and numerical tools for the study of waveguide discontinuities, planar transmission lines, and microwave filters. From 1993 to 1995, he was with the Space Division, Industry Alcatel Espacio, Madrid, Spain, and was also with the ESA, where he collaborated in several ESA/European Space Research and Technology Centre (ESTEC) contracts. From 1995 to 1999, he was with the Swiss Federal Institute of Technology, École Polytechnique Fédérale de Lausanne (EPFL), Lausanne, Switzerland, where he was involved with the field of microstrip antennas and printed circuits for space applications. In 2000, he joined the Technical University of Cartagena, Spain, where he is currently developing his teaching and research activities.

Dr. Alvarez Melcón was the recipient of the Journée Internationales de Nice Sur les Antennes (JINA) Best Paper Award for the best contribution to the JINA'98 International Symposium on Antennas, and the Colegio Oficial de Ingenieros de Telecomunicación (COIT/AEIT) Award to the best Ph.D. thesis in basic information and communication technologies.